Sequential extraction and DXRD applicability to poorly crystalline Fe and Al phase characterization from an Acid Mine Water Passive Remediation System.

Manuel A. Caraballo[1], Tobias S. Rötting[2], José Miguel Nieto[1] and Carlos Ayora[3]

1 Geology Department, University of Huelva, Campus "El Carmen", E-21071 Huelva, Spain

2 Newcastle University, Sir Joseph Swan Institute for Energy Research, Newcastle upon Tyne, NE1 7RU, United Kingdom

3 Institute of Environmental Assessment and Water Research, CSIC, Jordi Girona 18, E-08034 Barcelona, Spain

ABSTRACT

Fe and Al precipitates play a very important hydrochemical and environmental role in aquatic environments affected by acid mine drainage. Despite their great importance, the reliable

characterization of these precipitates usually presents many problems due to the high proportion of amorphous or poorly ordered mineral phases comprising these precipitates and because the coexistence with intermediate to highly crystalline phases. To facilitate and improve the characterization of poorly ordered Fe and Al phases, a coupled DXRD and sequential extraction study was performed on a set of samples from an acid mine water passive treatment system. By the use of these techniques, the presence of schwertmannite and goethite was shown in the upper 5 cm of the passive treatment reactive material. Furthermore, a progressive decrease of the $SO_4^{=}$ adsorbed to the schwertmannite surface also was suggested by one of the sequential extraction steps. Concerning the Al precipitates, the presence of hydrobasaluminite and gibbsite (as an aging product of the former) was also proposed on the basis of sequential extraction analysis. These techniques also allow a quantitative estimation of the proportion of each mineral. As a result, a complete study of the distribution of each mineral throughout the reactive material profile and the role of each phase in removing metals from the mine water can be obtained. This information is useful not only to improve the reactive material design but also to understand the natural processes taking place in aquatic systems affected by mining.

KEYWORDS

Sequential Extraction, DXRD, schwertmannite, hydrobasaluminite, gibbsite, acid mine drainage, passive treatment system.

INTRODUCTION

45 The hydrochemistry and mineralogy of waters affected by acid mine drainage (AMD) are
46 mainly controlled by SO_4-Fe and SO_4-Al systems at pH ranges between 1-5 and 5-6,
47 respectively (Bigham and Nordstrom, 2000).

48 Fe^{3+} hydrolysis tends to buffer AMD pH around 3.5 by the precipitation of schwertmannite
49 according to the reaction:

$$8Fe^{3+} + xSO_4^{2-} + (16-2x)H_2O \rightleftharpoons Fe_8O_8(OH)_{8-2x}(SO_4)_x + (24-2x)H^+ \quad (1)$$

50 where $1 \leq x \leq 1.86$, as shown by after Bigham et al. (1996) and Yu et al. (1999).

51 In the same way, Al^{3+} hydrolysis, with a $pK_1 = 5$ (Alpers et al., 2008), and subsequent
52 precipitation of hydrobasaluminite, $Al_4(SO_4)(OH)_{10}\cdot 15H_20$, buffers AMD pH around a value
53 of 5. This hydrolysis reaction can be written as follows:

$$4Al^{3+}_{(aq)} + SO_4^{2-}{}_{(aq)} + 25H_2O_{(l)} \rightleftharpoons Al_4(SO_4)(OH)_{10}\cdot 15H_20_{(s)} + 10H^+_{(aq)} \quad (2)$$

54 The mineralogical control that both phases have on AMD hydrochemistry is not only
55 restricted to pH buffering but also to some metal adsorption and coprecipitation processes.
56 Accordingly, schwertmannite has been observed to play an essential role in the adsorption of
57 As (Acero et al., 2006; Fukushi and Sverjensky, 2007) and also a main role in the adsorption
58 of Pb and Cu (Michel et al., 2007; Webster et al., 1998). Concerning hydrobasaluminite
59 adsorption processes, an important decrease in dissolved Cu and Cd have been reported in the
60 presence of this mineral (Sánchez-España et al., 2006).

61 Many studies have been developed using synthetic schwertmannite (Eskandarpour et al.,
62 2008; Loan et al., 2004) or pure natural schwertmannite especially collected from specific
63 AMD precipitates (Bigham et al., 1996; Kawano and Tomita, 2001; Yu et al., 1999).

64 However, the appearance of isolated schwertmannite in natural precipitates (Regenspurg et
65 al., 2004) or in passive treatment systems (Gagliano et al., 2004; Rötting et al., 2008) has been
66 reported as quite uncommon.

67 Being a metastable phase, schwertmannite tends to transform by aging into goethite (Bigham
68 et al., 1996; Burton et al., 2007; Jönsson et al., 2005; Knorr and Blodau, 2007), jarosite
69 (Wang et al., 2006) or both minerals (Acero et al., 2006), which implies that all these minerals
70 are commonly found coexisting in mixed precipitates.

71 The distribution and greater intensity of jarosite and goethite diffractogram peaks compared to
72 those of schwertmannite leads to a serious problem when a mixture of these minerals has to
73 be characterized by XRD because schwertmannite peaks are hidden by those of jarosite and
74 goethite. To solve this problem, Differential X-ray Diffraction (DRXD) can be used (Dold,
75 2003b; Schulze, 1981; Singh et al., 1999). Nevertheless, this technique is not completely
76 reliable for examining very poorly crystalline schwertmannite and sometimes needs to be
77 supported by other analytical techniques.

78 Hydrobasaluminite is also a poorly crystalline phase, whose XRD diffractogram is difficult to
79 relate with the mineral itself (Kim and Kim, 2003). Thus, if this mineral belongs to a
80 polymineral precipitate with more crystalline phases it is very difficult to detect even with
81 DXRD.

82 Recently some studies of poorly and moderately crystallized sulfate and oxide minerals have
83 been developed using new techniques like Visible Near-Infrared Reflectance (VNIR) (Alpers,
84 2008; Bishop, 2008), synchrotron XRD and XRF (Michel et al., 2007; Root et al., 2007) or X-
85 ray Absorption Near-Edge Structure (XANES) (Alpers et al., 2008; Bishop, 2008) and
86 Extended X-ray Absorption Fine Structure (EXAFS) (Alpers et al., 2008; Chen and Jiang,

2008). These studies determine not only the mineralogy of the sample but also the site occupied by the different elements in the mineral structure. However, these techniques are not easily available, thus it is desirable to have a previous general study of the samples for an efficient use of the beam time.

Sequential Extraction procedures (SE) are accessible and reliable techniques allowing a quantitative and qualitative mineralogical analysis of the sample but also a first insight into the elements distribution in the mineral structure. In this respect, the ability of many different sequential extraction procedures to elucidate the availability and general metal distribution on different mineral phases have been reliably demonstrated (Dold, 2003b; Fanfani et al., 1997; Pueyo et al., 2008; Rodríguez et al., 2008; Terzano et al., 2007). On the other hand, although some reported works have related the specific Fe-precipitate mineralogy with the different amounts of dissolved iron and sulfur obtained by sequential extraction procedures (Dold, 2003b; Fanfani et al., 1997; Hall et al., 1996; Li et al., 2007), it still remains necessary to perform new studies focused not only on Fe-oxide and Fe-sulfate minerals but also on Al-sulfate minerals.

Traditionally, studies about the interaction between AMD and passive treatment systems are focused on inflow and outflow water quality, paying no attention to detailed mineralogy developed inside the reactive material (Cocos et al., 2002; Jarvis et al., 2006; Johnson and Younger, 2006; Kalin, 2004; Kalin and Caetano Chaves, 2003; Laus et al., 2007; Sapsford et al., 2007; Shin et al., 2008). The objective of the present work is to test the applicability of a specific sequential extraction procedure and DXRD for the mineralogical characterization of AMD precipitates mainly formed by poorly ordered iron and aluminum oxides and sulfates. The Monte Romero passive treatment system (Rötting et al., 2008) was chosen as the best

110 place to carry out this study because inside its reactive material schwertmannite and
111 hydrobasaluminite precipitate, and the former ages to goethite. Within the passive treatment
112 system, it is possible to find all the intermediate steps between different hydrochemical
113 conditions during AMD neutralization.

114

115 **MATERIALS AND METHODS**

116 **Field Site and Sampling Description**

117 All samples used for this study were collected inside the reactive material of the Monte
118 Romero pilot scale passive treatment system in July 2006. At that time the system comprised
119 a cylindrical $3m^3$ reactive tank connected in series with three decantation ponds with an
120 approximate volume of $6m^3$ each. Dispersed Alkaline Substrate (DAS) (Rötting et al., 2008)
121 was used as the treatment reactive material. This substrate was prepared by mixing 25% (v/v)
122 calcite sand with 75% (v/v) pine wood chips.

123 The AMD emerging from one shaft of the Monte Romero underground mine was partially
124 collected and channelled to the reactive tank by polyethylene pipes. Prior to the treatment
125 operation, the AMD had a pH near 3.3, a net acidity of 1400–1600 mg/L as $CaCO_3$
126 equivalents and mean concentrations of 315 mg/L Fe (97% Fe(II)), 310 mg/L Zn, 270 mg/L
127 Ca, 75 mg/L Al, 20 mg/L Mn, 1.5 mg/L Cu and 3200 mg/L sulfate (Rötting et al., 2008).

128 During the vertical gravity flow of the AMD across the reactive material some hydrochemical
129 changes occur. Calcite dissolution causes a rise in pH and the subsequent precipitation of
130 schwertmannite (pH between 3 and 4.5) and Al-hydroxysulfates (at pH 5 to 5.5). The
131 precipitation of schwertmannite in the decantation pond consumes the excess of alkalinity,

produce by calcite dissolution inside the reactive material, also lowering water pH to values around 3-3.5, according to the reaction (1).

For the solid sampling, water flow was stopped and a 90cm cross section was dug to have a view of the different precipitate layers developed inside the reactive material. Six levels were macroscopically detected by visual changes in color, shape and texture of the precipitates: 1) a friable reddish-dark brown level from 0 to 1 cm, 2) a dark orange level from 1 to 3 cm, 3) a light orange-yellowish zone from 3 to 5 cm, 4) a white-pinkish cemented zone from 5 to 15 cm, 5) a yellowish zone from 15 to 30 cm and finally 6) the apparently unreacted substrate from 30 to 90 cm.

In accordance to that, seven samples were taken to characterize not only the precipitates but also the transition zones between the main precipitate layers. The selected depths were: 0-1, 1-3, 3-5, 5-15, 15-20, 20-30 and 30-40 cm.

Analytical Methods

As a first approach to the constituent mineralogy of the samples an X-ray diffraction (XRD) study of randomly oriented powder samples was performed using a Bruker D5005 X-ray Diffractometer with Cu Kα radiation. Diffractometer settings were: 40 kV, 30 mA and a scan range of 3–70º 2θ, 0.05º 2θ step size and 20-s counting time per step.

Differential X-ray diffraction (DXRD) is a suitable technique for determining the presence of poorly crystalline minerals in samples that contain a mixture of poorly to highly crystalline minerals. This technique involves the subtraction of a treated sample diffractogram from the diffractogram of the same sample prior to treatment (Schulze, 1981). The selective dissolution

of minerals changes the relative concentration of the remaining phases in the treated sample, therefore an intensity correction factor (k-factor) is applied to normalize both diffractograms during the subtraction.

The qualitative analysis of the different diffractograms obtained during this study was performed using XPowder (Version 2004.03), a software package for powder X-ray diffraction analysis.

In addition to the XRD and DXRD study, some gold coated samples and carbon coated polished sections were examined with a JEOL JSM-5410 scanning electron microscope (SEM) to observe the morphology of the constituent minerals. Energy dispersive spectrometry (EDS) was used to obtain a semi-quantitative compositional analysis of single crystals.

The metal concentrations of the different extractants obtained at each step of the sequential extraction were determined by Inductively Coupled Plasma Atomic Emission Spectrometry (ICP-AES Yobin-Ybon Ultima2). Every ten samples standards were used to check the accuracy. Due to the mineralogical approach of this study only Fe, Al, S and Ca will be presented, although some other metals were also measured. The detection limit for these four elements was always lower than 0.1 mg/L.

During the sequential extraction study some samples were duplicated in order to evaluate the procedure reproducibility.

Sequential Extraction Procedure

The four essential factors defining a sequential extraction procedure are: chemicals employed for the extractants, sample-extractant volume ratio, time and nature of the contact between the

176 solid sample and the extractant and environmental conditions during each step of the
177 extraction sequence.

178 For almost all the minerals concerning this study (gypsum, calcite, schwertmannite and
179 goethite) appropriate selective extractants and careful studies of experiment environmental
180 conditions have been conducted (Dold, 2003b; Fanfani et al., 1997; Hall et al., 1996;
181 Sahuquillo et al., 2003; Stumm and Sulzberger, 1992). However, to successfully apply these
182 studies to samples with high concentrations of iron oxides and iron oxyhydroxysulfates (e.g.
183 AMD Fe-stromatolites or Fe-precipitates from passive treatment systems) some changes to
184 the sample-extractant volume ratio and the time and nature of contact are needed.

185 No previous studies of hydrobasaluminite selective extractants have been reported. Therefore,
186 it was decided to subject the samples hosting this mineral to the specific sequential extraction
187 steps designed for Fe(III) minerals.

188 The different sequential extraction steps conducted in this study with the type and amount of
189 extractant, the amount of sample and the experiment environmental conditions are
190 summarized in Table 1. A more detailed explanation of the selected experimental conditions
191 and a brief description of the expected information offered by each step of the sequential
192 extraction is presented here.

193 *1) Water soluble fraction:* due to the importance of secondary sulfates and other salts in AMD
194 environments, an initial water extraction step is essential for a complete understanding of
195 these environments. This step has a double function, on the one hand the water composition
196 after dissolution of secondary sulfates and other salts reflects the portion of easily available
197 contaminants, on the other hand these minerals usually appear as well-crystalline phases

198 which is a problem if coexisting poorly crystalline phases are to be detected by XRD (the
199 most intense diffractogram peaks of the former mask the weaker peaks of the latter).

200 To ensure complete dissolution of all water-soluble minerals present in our samples, a twelve-
201 hour shaking period was selected.

202 *2) Sorbed and exchangeable fraction:* This step has an important role in the study of samples
203 with carbonate minerals (Fanfani et al., 1997; Hall et al., 1996; Tessier et al., 1979) because
204 the complete dissolution of calcite and other carbonates takes place during NH_4-acetate leach.
205 Due to the high crystallinity of these minerals a complete dissolution of them is necessary if a
206 DXRD for the study of poorly ordered phases is to be conducted.

207 This step also extracts elements that are adsorbed to mineral surfaces (Dold, 2003b; Hall et
208 al., 1996). This knowledge is essential to understand the distribution of some elements (e.g. S
209 as $SO_4^{=}$) in the structure of some minerals (schwertmannite, goethite and hydrobasaluminite
210 in our study), and is important to characterize the availability of some metals.

211 In this step the 1M NH_4-acetate solution was buffered to pH 4.5 by the addition of acetic acid.
212 To have an idea of the effect of reaction time on schwertmannite stability, two different
213 reaction times were employed during the sequential extraction calibration study: two hours for
214 sample A1 and one hour for samples A2-A5 (Fig.1). As can be observed, the reduction of the
215 reaction time implies a significant decrease on the dissolved iron for this step.

216 *3) Poorly ordered Fe (III) oxyhydroxides and oxyhydroxysulfates:* the specificity and well
217 documented behavior (Dold, 2003b; McCarty et al., 1998; Stumm and Sulzberger, 1992) of
218 0.2M NH_4-oxalate for schwertmannite dissolution makes this extractant the best candidate for
219 the study of our samples.

A deep and exhaustive study of the dissolution kinetics of schwertmannite and a proposal for two different sequential extraction steps focusing on the specific dissolution of schwertmannite and goethite can be found in Dold (2003a and b). Therefore, it was decided to use the proposed steps for schwertmannite and goethite selective dissolution; however, a preliminary study of the sample-extractant volume ratio was necessary to adjust that procedure to pure schwertmannite or samples with high schwertmannite content.

Five different ratios of solid sample: liquid extractant were selected (in mg/ml): 50:1, 10:1, 5:1, 2.5:1 and 1:1. The results of this calibration study (Fig.1) clearly show that the ratio 50:1 is too high to achieve the complete dissolution of schwertmannite during sequential extraction step three, with some schwertmannite remaining after the final digestion step. Although all the other ratios tested lead to the complete dissolution of schwertmannite in the third step of the sequential extraction, the total amount of extracted iron decrease observed with the solid:solution ratio. For this step of the extraction sequence, a ratio of 10:1 was selected to conduct the study of Monte Romero precipitates. Thirty minutes reaction time was selected, based on previous studies (Bigham et al., 1996; Dold, 2003b).

4) Highly ordered Fe (III) hydroxides and oxides: the study of more crystalline iron precipitates (goethite in this case) was carried out using a sequential extraction step presented previously by Dold (2003b). As in step 2 the extractant used was 0.2M NH_4-oxalate but in this case the samples were exposed to light and heated to 80ºC in a water bath.

During the different sequential extraction experiments carried out for this study, it was observed that the complete dissolution of goethite took place after thirty minutes of digestion. Therefore, the sample-extractant contact time for this step was set to one hour to ensure complete goethite dissolution.

5) Residue digestion: after the first four sequential extraction steps, the samples used in this study consist almost completely of residual organic material (wood chips) with no expected mineral remaining, with the possible exception of a small residual fraction of detrital and atmospheric particulate (quartz and clays). In accordance to that, the digestion procedure developed for the total digestion of samples with organic and inorganic compounds were selected (Querol et al., 1996). The different acids used at this digestion were HF, to ensure the complete dissolution of the inorganic materials, and $HClO_4$ and HNO_3 dissolving the organic material.

RESULTS AND DISCUSSION

Mineralogical characterization of the reactive tank

As explained above, six different levels were visually detected during the sampling of Monte Romero DAS-reactive material.

Layer 1: (0-1 cm, friable, reddish-dark brown) this thin layer is developed at the contact between the supernatant AMD and the DAS-reactive material, where the solution pH is between 3 and 4 (Rötting et al., 2008). At this pH range and with the metal composition of this water it is reasonable to assume that schwertmannite is the main precipitate mineral. Another important observation was the complete absence of wood chips in the precipitates that suggests an upward growth of this layer (from the surface of the reactive material to the supernatant water).

The first XRD approach to the mineralogical composition of this layer showed a very weak diffractogram with a broad peak centered at 35º 2□ and a clearer 4.18 Å goethite peak (Fig. 2, raw sample). To resolve the different peaks belonging to this 35º centered broad peak, the

266 samples were submitted to all the steps of the sequential extraction procedure taking away a
267 subsample for XRD analysis at steps 2 and 3. As shown in figure 2, after NH_4-acetate attack
268 (step 2) the diffractogram pattern of the sample remained unaltered. However, when the
269 sample was treated with oxalate (step 3) the diffractogram pattern was substantially altered,
270 and a clear and well-defined goethite diffractogram appears.

271 To determine which phases were dissolved in the sequential steps, a DXRD study was
272 conducted using diffractograms of the raw sample and that after S.E. step 3. A K-factor of
273 0.8 was applied to the step-3 diffractogram to normalize the relative mineral concentration of
274 both samples. The resulting diffractogram is shown in left upper part of Fig. 2 where the
275 presence of schwertmannite was revealed by a well-defined 2.54 Å peak.

276 Although this observation seems to reliably determine the presence of schwertmannite, it is
277 not completely conclusive because 2-line ferrihydrite has its main diffractogram peak at 2.54
278 Å and is selectively dissolved by NH_4-oxalate as well (Dold, 2003b). To resolve this issue, a
279 SEM-EDS analysis of the sample was carried out where both images of the characteristic
280 "pincushion" or "sea-urchin" morphology of schwertmannite and semi-quantitative chemical
281 analysis were obtained (Fig. 2).

282 For the sequential extraction analysis, a summary of Fe, Al, S and Ca concentrations for each
283 sample, obtained at the different sequential extraction steps, is presented in Fig. 3. More than
284 a 75% of the total iron was released in step 3. Schwertmannite probably is the mineral phase
285 responsible for most of the iron removed from this layer. Examination of the S released
286 throughout the sequential extraction steps revealed that 72% of the schwertmannite S was put
287 into solution in step 2, while the 28% remaining was released during step 3. Taking into
288 account this observation and similarity of the diffractograms of raw and step-2 samples, it can

289 be reliably assumed that no crystalline phase was dissolved during step 2. The amount of S
290 extracted in step 2 suggests that 72% of schwertmannite compositional S is adsorbed to the
291 mineral surface while only 28% is strongly fixed within the crystal structure. This double
292 distribution of S (as $SO_4^{2=}$) at the surface and in the inner structure of schwertmannite has
293 been previously reported (Bigham et al., 1990; Jönsson et al., 2005; Webster et al., 1998),
294 however, the amount of adsorbed S reported by them ranged from 30-35% (Bigham et al.,
295 1990; Jönsson et al., 2005) to as high as 60% (Webster et al., 1998), but not as high as the
296 72% found here. The adsorption of $SO_4^{=}$ also has been reported to take place at the surface of
297 goethite, but always at nearly insignificant levels when schwertmannite is present (Fukushi
298 and Sverjensky, 2007; Webster et al., 1998).

299 The $(Fe/S)_{molar}$ ratio of schwertmannite present in the different representative samples of the
300 iron precipitation zone and the resulting schwertmannite compositional formula for each
301 sample are shown in Table 2. The $(Fe/S)_{molar}$ ratio of 4.44 and the schwertmannite
302 stoichiometry, $Fe_8O_8(OH)_{4.4}(SO_4)_{1.8}$, obtained for this sample are identical to the values
303 obtained for the precipitates forming in terraces surrounding the Monte Romero shaft (Acero
304 et al., 2006). Schwertmannite sulfate stoichiometry of this sample is higher than the one
305 proposed by Bigham et al. (1996), but in good agreement with the range of 1.74-1.86
306 suggested by Yu et al.(1999).

307 *Layer 2: (1-3 cm, dark orange-brown)* this level was the first one developed inside the DAS-
308 reactive material. The XRD analysis for the raw sample (Fig.4) clearly showed the presence
309 of goethite and also suggested the presence of gypsum whereas almost no peaks of
310 schwertmannite were detected. But, subsequently, when the DXRD analysis was performed

311 using sample 1-3 cm after step 2 (to avoid the presence of gypsum) and after step 3, with a K-
312 value of 0.85, the occurrence of schwertmannite was revealed (Fig.4).

313 The sequential extraction analysis for this sample revealed a very similar schwertmannite
314 composition compared to the schwertmannite from layer 0-1 cm (Fig.3), showing 75%
315 adsorbed $SO_4^{=}$ and a $(Fe/S)_{molar}$ ratio of 4.15 (Table 2). On the basis of released S and Ca in
316 step 1, gypsum can be assumed as a new mineral phase appearing at this level. This
317 observation is supported by the previously reported presence of this mineral in the raw sample
318 diffractogram and by the disappearance of this peak in the 1-3 cm diffractogram following
319 sequential extraction step 1.

320 *Layer 3: (3-5 cm, light orange-yellowish)* according to the hydrochemical profile and the
321 reactive transport model reported previously (Rötting et al., 2008) this layer corresponds to a
322 hydrochemical transition zone between Fe-rich and Al-rich precipitates, thus any of the
323 mineral phases found in this study could be present in this layer. Initial XRD analyses of the
324 constituent mineral phases of this layer (Fig. 5) revealed the unequivocal presence of goethite,
325 gypsum and calcite, although no peaks of schwertmannite or hydrobasaluminite were
326 observed even with DXRD.

327 Although the presence of schwertmannite could not be confirmed by the used of X-ray
328 techniques, the amount of iron released in step 3 (Fig.3) suggested the presence of a small
329 amount of this mineral. Examination of released S in step 2 revealed an important decrease of
330 adsorbed $SO_4^{=}$ compared to the concentrations found in the upper levels of the reactor. If
331 schwertmannite occurs in this layer, the $(Fe/S)_{molar}$ ratio (9.33) and the stoichiometry
332 $(Fe_8O_8(OH)_{6.28}(SO_4)_{0.86})$ are different in this level than elsewhere in the reactor. This is the
333 first level in which the presence of calcite has been reported (Fig.5). Taking into account this

observation, it is reasonable to assume that due to the presence of this calcite the pH of the AMD at this point is higher compare to layer 2. As a result of this pH increase, the surface of schwertmannite was partially occupied by OH^- anions, which compete for adsorption sites with $SO_4^=$ (Langmuir, 1997).

Examination of the aluminum concentrations obtained in the sequential extraction revealed, as expected, a small increase of this element in this layer (Fig.3). Due to the great variety of minerals precipitated in this level and the small amount of Al-precipitates present, a determination of the specific mineral phases responsible for the Al removal was impossible even with sequential extraction data. However, on the basis of the hydrochemical data of a previous study (Rötting et al., 2008) and according to the literature (Bigham and Nordstrom, 2000; Nordstrom, 1982; Sánchez-España et al., 2006; Sánchez-España and Trevor, 2007) hydrobasaluminite is shown as the most probable Al-phase precipitated within this layer.

Layer 4: (5-15 cm, "cemented", white-pinkish) when this layer was sampled, a significant amount of white-pinkish precipitates filling substrate pores and on surfaces of calcite and wood chips was observed. The presence of these precipitates cemented the reactive material in the DAS layer.

As shown in Fig. 5, only gypsum and calcite were detected by XRD in this layer. The fact that a large amount of aluminum was removed from solution in this level (Rötting et al., 2008) suggests that some poorly ordered or amorphous Al-phases must be present. This hypothesis is also supported by SEM-EDS observations (Fig.6), where gypsum and an Al-hydroxysulfate were seen to be closely precipitated around calcite grains. In some cases, it appears that excess Ca due to calcite dissolution promotes gypsum precipitation at its surface (Booth et al., 1997; Rötting et al., 2008) with a later Al-hydroxysulfate precipitation on top (Fig.6 A-B). By

contrast, direct precipitation of Al-hydroxysulfate on calcite surfaces (Fig.6 A) has also been observed, suggesting that both Al-hydroxysulfate and gypsum can precipitate directly on the calcite surface.

In the sequential extraction of this sample, an important amount of Al was released during step 3. The molar ratio of aluminum to sulfur in this level was as high as 16 while the theoretical Al/S molar ratio for hydrobasaluminite is 4. This result suggests the presence of at least two Al-phases. Some studies have reported the coexistence of basaluminite and gibbsite (Nordstrom, 1982) and the presence of gibbsite as an aging product of other metastable Al-phases (Berkowitz et al., 2006; Berkowitz et al., 2005; Nordstrom, 1982; Sims and Ellis, 1983). In addition, the presence of amorphous to microcrystalline gibbsite also has been reported in different environments (Berkowitz et al., 2005; Bigham and Nordstrom, 2000; Nordstrom, 1982; Nordstrom and Ball, 1986). These results, combined with the long treatment period during which schwertmannite ages to goethite, also suggests that hydrobasaluminite could be aging to gibbsite in this level.

Assuming the coexistence of hydrobasaluminite and gibbsite, Al distribution in these phases was calculated (Table 3), using theoretical formulas of hydrobasaluminite, $Al_4(SO_4)(OH)_{10}\cdot 15H_20$, and gibbsite, $Al(OH)_3$. The proportion of Al in hydrobasaluminite, was calculated as four times the amount of S released in steps 2-3 S (according to hydrobasaluminite stoichiometry). Aluminum in gibbsite was calculated as the remaining amount after subtracting hydrobasaluminite Al from total Al.

Layer 5: (15-20 cm and 20-30 cm, yellowish) this layer was selected based on its color and texture as a different precipitate layer, however XRD and sequential extraction analysis revealed that, this layer represents the progressive transition from the upper part of the Al-

precipitates level to the unreacted material. As in layer 4, the presence of gypsum and calcite was detected by XRD (Fig. 5) and the appearance of hydrobasaluminite and gibbsite is suggested by the sequential extraction analysis (Fig. 3 and Table 3), although in this case the amount of precipitates decreases dramatically from the top of this layer towards the unreacted material below.

Layer 6: (30-40 cm, apparently unreacted substrate) as expected, this layer corresponds to the unreacted original material where only the presence of calcite was detected by XRD (Fig. 5) and sequential extraction analysis (Fig. 3).

General distribution of the precipitates inside the reactive tank

The distribution of precipitates and the role of each mineral in metal removal is synthesized in Fig. 7. The right side of this figure shows the amount of total Fe, Al, S and Ca obtained by each step of the sequential extraction. The left side of the figure shows the concentration (weight %) of the different minerals found in each level. Inspection of these metal and mineralogical profiles (Fig. 7) clearly shows the presence of two distinct Fe and Al precipitation levels with a coexisting gypsum level.

Detailed inspection of the Fe level (0-5 cm) shows that although the amount of goethite in the samples was considerably greater than that of schwertmannite, the latter was the mineral phase responsible for most of the iron removal, because each mg of schwertmannite has eight times more iron than a mg of goethite due to each mineral stoichiometry. This mineral proportion also was observed in the XRD analyses for sample 0-1, 1-3 and 3-5 cm (Fig. 2, 4 and 5), where detection of schwertmannite prior to DXRD analysis was impossible due both to the lower crystallinity and concentration of schwertmannite with respect to goethite. The

amount of precipitated iron progressively decreased from the top to the bottom of the Fe level. Another important result of the sequential extraction study of the iron levels (Fig. 3) was the progressive decrease of $SO_4^{=}$ adsorbed onto schwertmannite with depth. This cannot be displayed in Figure 7b because $SO_4^{=}$ adsorption is overprinted by gypsum precipitation.

Gypsum was found throughout the reactor system, however, a detail inspection of the analyses showed that this mineral formed almost an independent level superimposed on the Fe and Al levels. From the results of S dissolved in step 1 of the sequential extraction (Fig. 3), the concentration of gypsum increases throughout the Fe level until reaches its maximum at the boundary between the Fe and Al level, and it decreases downward through the Al level.

The distribution of Al precipitates has a number of similarities to the distribution of Fe precipitates. In both cases, a mineral produced on aging (gibbsite or goethite) is more abundant than the metastable phase (hydrobasaluminite or schwertmannite). Also in both cases, the amount of metal removal progressively decreased from the top to the bottom of the layer (Fig. 7). However, an important difference between the Fe and Al layers is that more Al is present in the stable phase (gibbsite) whereas more iron is present in the metastable phase (schwertmannite; Table 3).

Another important observation offered by the sequential extraction analysis was the amount of calcite consumed in the different depths of the reactive material. Inspection of the amount of Ca released during the second step of the sequential extraction (Fig. 3) revealed that almost all the calcite was consumed in the Fe level (0-5 cm) while an important amount of calcite remained undissolved in the Al level. The distribution of calcite in the Al level showed the same decreasing tendency from 15 to 30 cm as shown by the Al precipitates. This fact could be explained by a calcite passivation process as the precipitation of Al-bearing minerals

shields the calcite surface, rendering it inaccessible to the solution. This passivation hypothesis is also supported by SEM-EDS results (Fig. 6) previously discussed.

CONLUSIONS

A combined use of sequential extraction and differential x-ray diffraction (DXRD) to study poorly ordered Al and Fe phases has been tested on precipitates formed inside the reactive material of the Monte Romero passive treatment system in southwestern Spain. This passive treatment system is being tested as a possible remediation method for acid mine drainage. The presence of schwertmannite and goethite was detected in the upper level of the treatment system, based on coupled sequential extraction and DXRD analyses. The stoichiometry of schwertmannite changed throughout the Fe level, and the amount of $SO_4^{=}$ adsorbed to schwertmannite decreased progressively downward through the Fe level, as determined from the sequential extraction results.

Gypsum distribution throughout the reactive material was determined on the basis of S released in the first step of the sequential extraction. Gypsum was present throughout the entire precipitation profile and it coexisted with both the Fe and Al levels (with gypsum precipitation maximum coincident with the boundary between the Fe and Al levels). This gypsum distribution could be the result of gypsum formation by combination of Ca increase by calcite dissolution with $SO_4^{=}$ in the acidic mine drainage.

The mineral concentrations interpreted from the sequential extraction facilitate an understanding of the general distribution of each mineral phase that forms within the reactive material and also to quantify the importance of each mineral on metal removal. These results

449 also can be used to infer the hydrochemical processes occurring inside the reactive material,
450 which is essential to improve the system quality and efficiency.

451 **AKNOWLEDGMENTS**

452 This study was funded by the Spanish Government projects REN-2003-09590-C04,
453 CTM2006-28151-E/TECNO and CTM2007-66724-C02.

454 M.A.C. was financially supported by the Spanish Government with PhD fellowship. We are
455 grateful to Patricia Acero from University of Zaragoza for the fruitful discussions and help.
456 We would also like to thank the analytical assistance of Rafael Carrasco and Mari Paz Martín
457 from the Central Research Services of the University of Huelva.

458

459 **REFERENCES**

460 Acero, P., Ayora, C., Torrentó, C., and Nieto, J.-M. (2006) The behavior of trace elements
461 during schwertmannite precipitation and subsequent transformation into goethite and
462 jarosite. Geochimica et Cosmochimica Acta, 70(16), 4130-4139.

463 Alpers, C.N., Majzlan, J., Bender, K.C., Bishop, J.L., Coleman, M.L., Dyar, M.D.,
464 McCleskey, R.B., Myneni, S.C.B., Nordstrom, D.K., and Sobron, P. (2008a)
465 Chemistry and spectroscopy of iron-sulfate minerals from Iron Mountain, California,
466 U.S.A. Geochimica et Cosmochimica Acta, 72(12, Supplement 1), A17.

467 Alpers, C.N., M.J., Bender Koch C, Bishop JL, Coleman ML, Dyar MD, McCleskey RB,
468 Myneni SCB, Nordstrom DK & Sobron P. (2008b) Chemistry and Spectroscopy of
469 Iron-Sulfate Minerals from Iron Mountain, California, U.S.A. Geochimica et
470 Cosmochimica Acta, 72(12, Supplement 1), A17.

471 Berkowitz, J., Anderson, M.A., and Amrhein, C. (2006) Influence of aging on phosphorus
472 sorption to alum floc in lake water. Water Research, 40(5), 911-916.
473 Berkowitz, J., Anderson, M.A., and Graham, R.C. (2005) Laboratory investigation of
474 aluminum solubility and solid-phase properties following alum treatment of lake
475 waters. Water Research, 39(16), 3918-3928.
476 Bigham, J.M., and Nordstrom, D.K. (2000) Iron and Aluminum Hydroxysulfates from Acid
477 Sulfate Waters. In C.N. Alpers, J.L. Jambor, and D.K. Nordstrom, Eds. Sulfate
478 Minerals: Crystallography, Geochemistry, and Environmental Significance, 40, p.
479 351-403. Reviews in Mineralogy and Geochemistry, Mineralogical Society of
480 America., Chantilly, Virginia.
481 Bigham, J.M., Schwertmann, U., Carlson, L., and Murad, E. (1990) A poorly crystallized
482 oxyhydroxysulfate of iron formed by bacterial oxidation of Fe(II) in acid mine waters.
483 Geochimica et Cosmochimica Acta, 54(10), 2743-2758.
484 Bigham, J.M., Schwertmann, U., Traina, S.J., Winland, R.L., and Wolf, M. (1996)
485 Schwertmannite and the chemical modeling of iron in acid sulfate waters. Geochimica
486 et Cosmochimica Acta, 60(12), 2111-2121.
487 Bishop J, A.C., Coleman M, Sobron P, Lane M, Dyar D & Schiffman P. (2008) Sulfates on
488 Mars: Comparison with Spectral Properties of Analog Sites. Geochimica et
489 Cosmochimica Acta, 72(12, Supplement 1), A85.
490 Booth, J., Hong, Q., Compton, R.G., Prout, K., and Payne, R.M. (1997) Gypsum overgrowths
491 passivate calcite to acid attack. J. Colloid Interf. Sci. , 192, 207-214.
492 Burton, E.D., Bush, R.T., Sullivan, L.A., and Mitchell, D.R.G. (2007) Reductive
493 transformation of iron and sulfur in schwertmannite-rich accumulations associated

494 with acidified coastal lowlands. Geochimica et Cosmochimica Acta, 71(18), 4456-
495 4473.
496 Chen, C.J., and Jiang, W.T. (2008) An EXAFS and FTIR Study on the Sulfate and Arsenate
497 Configurations of Schwertmannite. Geochimica et Cosmochimica Acta, 72(12,
498 Supplement 1), A152.
499 Cocos, I.A., Zagury, G.J., Clément, B., and Samson, R. (2002) Multiple factor design for
500 reactive mixture selection for use in reactive walls in mine drainage treatment. Water
501 Research, 36(1), 167-177.
502 Dold, B. (2003a) Dissolution kinetics of schwertmannite and ferrihydrite in oxidized mine
503 samples and their detection by differential X-ray diffraction (DXRD). Applied
504 Geochemistry, 18(10), 1531-1540.
505 -. (2003b) Speciation of the most soluble phases in a sequential extraction procedure adapted
506 for geochemical studies of copper sulfide mine waste. Journal of Geochemical
507 Exploration, 80(1), 55-68.
508 Eskandarpour, A., Onyango, M.S., Ochieng, A., and Asai, S. (2008) Removal of fluoride ions
509 from aqueous solution at low pH using schwertmannite. Journal of Hazardous
510 Materials, 152(2), 571-579.
511 Fanfani, L., Zuddas, P., and Chessa, A. (1997) Heavy metals speciation analysis as a tool for
512 studying mine tailings weathering. Journal of Geochemical Exploration, 58(2-3), 241-
513 248.
514 Fukushi, K., and Sverjensky, D.A. (2007) A surface complexation model for sulfate and
515 selenate on iron oxides consistent with spectroscopic and theoretical molecular
516 evidence. Geochimica et Cosmochimica Acta, 71(1), 1-24.

517 Gagliano, W.B., Brill, M.R., Bigham, J.M., Jones, F.S., and Traina, S.J. (2004) Chemistry and
518 mineralogy of ochreous sediments in a constructed mine drainage wetland.
519 Geochimica et Cosmochimica Acta, 68(9), 2119-2128.
520 Hall, G.E.M., Vaive, J.E., Beer, R., and Hoashi, M. (1996) Selective leaches revisited, with
521 emphasis on the amorphous Fe oxyhydroxide phase extraction. Journal of
522 Geochemical Exploration, 56(1), 59-78.
523 Jarvis, A.P., Moustafa, M., Orme, P.H.A., and Younger, P.L. (2006) Effective remediation of
524 grossly polluted acidic, and metal-rich, spoil heap drainage using a novel, low-cost,
525 permeable reactive barrier in Northumberland, UK. Environmental Pollution, 143(2),
526 261-268.
527 Johnson, K.L., and Younger, P.L. (2006) The co-treatment of sewage and mine waters in
528 aerobic wetlands. Engineering Geology, 85(1-2), 53-61.
529 Jönsson, J., Persson, P., Sjöberg, S., and Lövgren, L. (2005) Schwertmannite precipitated
530 from acid mine drainage: phase transformation, sulphate release and surface
531 properties. Applied Geochemistry, 20(1), 179-191.
532 Kalin, M. (2004) Passive mine water treatment: the correct approach? Ecological
533 Engineering, 22(4-5), 299-304.
534 Kalin, M., and Caetano Chaves, W.L. (2003) Acid reduction using microbiology: treating
535 AMD effluent emerging from an abandoned mine portal. Hydrometallurgy, 71(1-2),
536 217-225.
537 Kawano, M., and Tomita, K. (2001) Geochemical modeling of bacterially induced
538 mineralization of schwertmannite and jarosite in sulfuric acid spring water. American
539 Mineralogist, 86(10), 1156-1165.

Kim, J.J., and Kim, S.J. (2003) Environmental, Mineralogical, and Genetic Characterization of Ochreous and White Precipitates from Acid Mine Drainages in Taebaeg, Korea. Environ. Sci. Technol., 37(10), 2120-2126.

Knorr, K.-H., and Blodau, C. (2007) Controls on schwertmannite transformation rates and products. Applied Geochemistry, 22(9), 2006-2015.

Langmuir, D. (1997) Aqueous environmental geochemistry. Prentice-Hall, Inc., New Jersey.

Laus, R., Geremias, R., Vasconcelos, H.L., Laranjeira, M.C.M., and Fávere, V.T. (2007) Reduction of acidity and removal of metal ions from coal mining effluents using chitosan microspheres. Journal of Hazardous Materials, 149(2), 471-474.

Li, J., Smart, R.S.C., Schumann, R.C., Gerson, A.R., and Levay, G. (2007) A simplified method for estimation of jarosite and acid-forming sulfates in acid mine wastes. Science of The Total Environment, 373(1), 391-403.

Loan, M., Cowley, J.M., Hart, R., and Parkinson, G.M. (2004) Evidence on the structure of synthetic schwertmannite. American Mineralogist, 89(11-12), 1735-1742.

McCarty, D.K., Moore, J.N., and Marcus, W.A. (1998) Mineralogy and trace element association in an acid mine drainage iron oxide precipitate; comparison of selective extractions. Applied Geochemistry, 13(2), 165-176.

Michel, F.M., Ehm, L., Sytle, M.A., Lee, P.L., Chupas, P.J., Liu, G., Strongin, D.R., Schoonen, M.A.A., Phillips, B.L., and Parise, J.B. (2007) The Structure of Ferrihydrite, a Nanocrystalline Material. Science, 316, 1726.

Nordstrom, D.K. (1982) The effect of sulfate on aluminum concentrations in natural waters: some stability relations in the system Al2O3-SO3-H2O at 298 K. Geochimica et Cosmochimica Acta, 46(4), 681-692.

563 Nordstrom, D.K., and Ball, J.W. (1986) The geochemical behaviour of aluminum in acidified
564 surface waters. Science, 232, 54-56.
565 Pueyo, M., Mateu, J., Rigol, A., Vidal, M., López-Sánchez, J.F., and Rauret, G. (2008) Use of
566 the modified BCR three-step sequential extraction procedure for the study of trace
567 element dynamics in contaminated soils. Environmental Pollution, 152(2), 330-341.
568 Querol, X., Alastuey, A., Lopez-Soler, A., Mantilla, E., and Plana, F. (1996) Mineral
569 composition of atmospheric particulates around a large coal-fired power station.
570 Atmospheric Environment, 30(21), 3557-3572.
571 Regenspurg, S., Brand, A., and Peiffer, S. (2004) Formation and stability of schwertmannite
572 in acidic mining lakes. Geochimica et Cosmochimica Acta, 68(6), 1185-1197.
573 Rodríguez, L., Ruiz, E., Alonso-Azcárate, J., and Rincón, J. (2008) Heavy metal distribution
574 and chemical speciation in tailings and soils around a Pb-Zn mine in Spain. Journal of
575 Environmental Management, In Press, Corrected Proof.
576 Root, R.A., Dixit, S., Campbell, K.M., Jew, A.D., Hering, J.G., and O'Day, P.A. (2007)
577 Arsenic sequestration by sorption processes in high-iron sediments. Geochimica et
578 Cosmochimica Acta, 71(23), 5782-5803.
579 Rötting, T.S., Caraballo, M.A., Serrano, J.A., Ayora, C., and Carrera, J. (2008) Field
580 application of calcite Dispersed Alkaline Substrate (calcite-DAS) for passive
581 treatment of acid mine drainage with high Al and metal concentrations. Applied
582 Geochemistry, 23(6), 1660-1674.
583 Sahuquillo, A., Rigol, A., and Rauret, G. (2003) Overview of the use of leaching/extraction
584 tests for risk assessment of trace metals in contaminated soils and sediments. TrAC
585 Trends in Analytical Chemistry, 22(3), 152-159.

586 Sánchez-España, J., Pamo, E., Pastor, E., Andrés, J., and Rubí, J. (2006) The Removal of
587 Dissolved Metals by Hydroxysulphate Precipitates during Oxidation and
588 Neutralization of Acid Mine Waters, Iberian Pyrite Belt. Aquatic Geochemistry, 12(3),
589 269-298.
590 Sánchez-España, J., and Trevor, M.L. (2007) The Behavior of Iron and Aluminum in Acid
591 Mine Drainage: Speciation, Mineralogy, and Environmental Significance.
592 Thermodynamics, Solubility and Environmental Issues, p. 137-150. Elsevier,
593 Amsterdam.
594 Sapsford, D., Barnes, A., Dey, M., Williams, K., Jarvis, A., and Younger, P. (2007) Low
595 Footprint Passive Mine Water Treatment: Field Demonstration and Application. Mine
596 Water and the Environment, 26(4), 243-250.
597 Schulze, D.G. (1981) Identification of soil iron oxides minerals by differential X-ray
598 diffraction. Soil Science Society of America Journal 45, 437- 440.
599 Shin, E.-J., Lauve, A., Carey, M., Bukovsky, E., Ranville, J.F., Evans, R.J., and Herring,
600 A.M. (2008) The development of bio-carbon adsorbents from Lodgepole Pine to
601 remediate acid mine drainage in the Rocky Mountains. Biomass and Bioenergy, 32(3),
602 267-276.
603 Sims, J.T., and Ellis, B.G. (1983) Changes in phosphorous sorption associated with aging of
604 aluminum hydroxide suspensions. Soil Sci. Soc. Am. J. , 47 (5), 912-916.
605 Singh, B., Wilson, M.J., McHardy, W.J., Fraser, A.R., and Merrington, G. (1999) Mineralogy
606 and chemistry of ochre sediments from an acid mine drainage near a disused mine in
607 Cornwall, UK. Clay Minerals, 34(2), 301-317.

608 Stumm, W., and Sulzberger, B. (1992) The cycling of iron in natural environments:
609 considerations based on laboratory studies of heterogeneous redox processes.
610 Geochimica et Cosmochimica Acta, 56, 3233- 30257.
611 Terzano, R., Spagnuolo, M., Vekemans, B., DeNolf, W., Janssens, K., Falkenberg, G., Fiore,
612 S., and Ruggiero, P. (2007) Assessing the Origin and Fate of Cr, Ni, Cu, Zn, Pb, and V
613 in Industrial Polluted Soil by Combined Microspectroscopic Techniques and Bulk
614 Extraction Methods. Environ. Sci. Technol., 41(19), 6762-6769.
615 Tessier, A., Campbell, P.G.C., and Bisson, M. (1979) Sequential extraction procedure for
616 speciation of particulate trace metals. Analytical Chemistry 51, 844-851.
617 Wang, H., Bigham, J.M., and Tuovinen, O.H. (2006) Formation of schwertmannite and its
618 transformation to jarosite in the presence of acidophilic iron-oxidizing
619 microorganisms. Materials Science and Engineering: C, 26(4), 588-592.
620 Webster, J.G., Swedlund, P.J., and Webster, K.S. (1998) Trace Metal Adsorption onto an
621 Acid Mine Drainage Iron(III) Oxy Hydroxy Sulfate. Environ. Sci. Technol., 32(10),
622 1361-1368.
623 Yu, J.-Y., Heo, B., Choi, I.-K., Cho, J.-P., and Chang, H.-W. (1999) Apparent solubilities of
624 schwertmannite and ferrihydrite in natural stream waters polluted by mine drainage.
625 Geochimica et Cosmochimica Acta, 63(19-20), 3407-3416.
626

627 **TABLES**

628 TABLE 1. Sequential extraction procedure developed for this study.

629

630 TABLE 2. Comparison between schwertmannite formula and $(Fe/S)_{molar}$ ratio proposed in the
631 literature and schwertmannite formula and $(Fe/S)_{molar}$ ratio obtained in this study.

632

633 TABLE 3. Deduced distribution of Al between hydrobasaluminite and gibbsite on the basis of
634 steps 2-3 S and total Al.

635 **FIGURE CAPTIONS**

636 Figure 1. Iron concentration obtained in the different steps of the sequential extraction
637 calibration study carried out for the 0-1 cm sample. Solid:extractant ratios in mg/ml.

638

639 Figure 2. Mineralogical characterization of sample 0-1 cm by XRD, DXRD and SEM-EDS.
640 Gt = Goethite, Sch = Schwertmannite.

641

642 Figure 3. Distribution of Fe, Al, S and Ca concentrations throughout the sample profile on the
643 basis of the sequential extraction study.

644

645 Figure 4. Mineralogical characterization by XRD and DXRD of sample 1-3 cm. Gt =
646 Goethite, Sch = Schwertmannite, Gyp =Gypsum.

647

648 Figure 5. XRD diffractograms for samples from 3-5 cm and 30-40 cm. The most important
649 peaks for the different mineral phases found in each sample have been labelled. Gt =
650 Goethite, Gyp = Gypsum, Cc = Calcite.

651

652 Figure 6. A) SEM image of a calcite grain surrounded by hydrobasaluminite (gray) and
653 gypsum (bright white) precipitates. B) Euhedral crystals of gypsum (centre) and amorphous
654 precipitates of hydrobasaluminite (lower-right corner of the image). At the bottom of these

655 two images three EDS elemental spectra (calcite = “cc”, gypsum = “gy”, and
656 hydrobasaluminite = “hyb”) obtained for some of the detected minerals are shown.
657
658 Figure 7. Metal (right diagram) and mineral (left diagram) distribution across the Monte
659 Romero reactive tank profile. Gt = Goethite, Sch = Schwertmannite, Gyp =Gypsum, Hybas =
660 Hydrobasaluminite, Gibb = Gibbsite, Cc = Calcite. The different areas drawn on the right
661 diagram correspond to the amount of each element attributed to the individual mineral phases.
662
663

664

TABLE 1. Sequential extraction procedure developed for this study

Sequential extraction step	Preferentially dissolved minerals	Dissolved phases (in this study)	Elements released to the solution
1) Water soluble fraction: 200 mg of sample into 20 ml deionizied water, shake for 12 h at room temperature (RT)	Secondary sulfates and other salts	Gypsum	Ca and SO_4^{2-}
2) Sorbed and exchangeable fraction: 20 ml of 1 M NH_4-acetate (4.5 pH buffer), shake for 1 h at RT	Calcite and some clay minerals	Calcite	Ca and adsorbed elements
3) Poorly ordered Fe (III) oxyhydroxides and oxyhydroxysulfates: 20 ml of 0.2 M NH_4-oxalate (3 pH buffer) 30 minutes shake in darkness and at RT	Mainly Schwertmannite and 2-line ferrihydrite	Schwertmannite, hydrobasaluminite and gibbsite	Fe, Al and SO_4^{2-}
4) Highly ordered Fe (III) hydroxides and oxides: 20 ml of 0.2 M NH_4-oxalate (3 pH buffer) 80 ºC water bath for 1h	Goethite, jarosite, 6-line ferrihydrite and hematite	Goethite	Fe
5) Residue digestion: 3 ml of HNO_3 + 7.5 ml of HF + 2.5 ml of $HClO_4$	Silicates	Residue (wood chips)	Organic elements

665
666
667
668
669

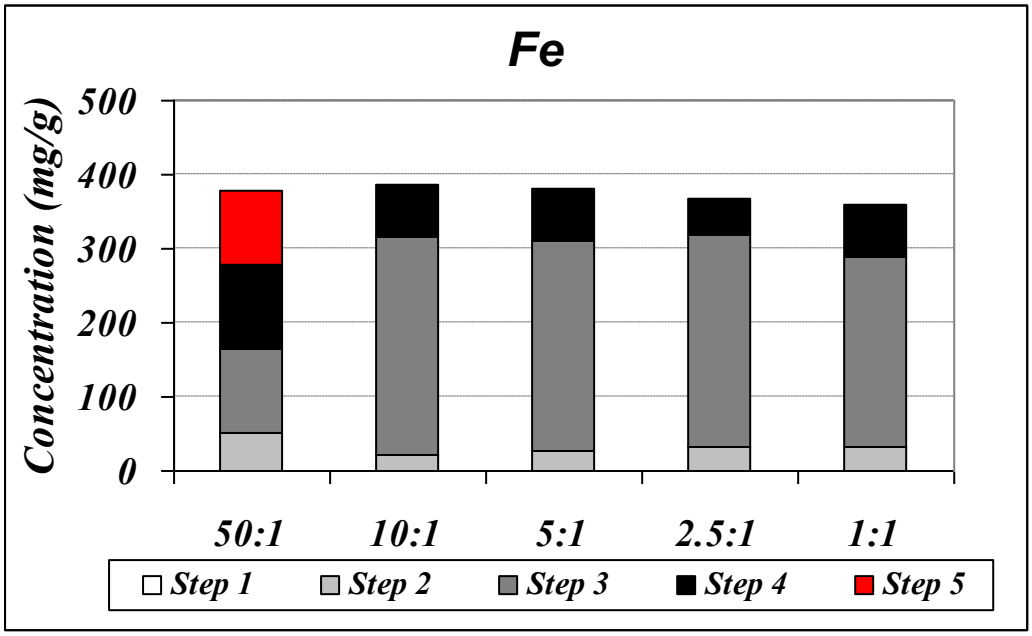

670
671 **FIGURE 1.** Iron concentration obtained in the different steps of the sequential extraction calibration study carried out for the 0-1 cm sample.

672 Solid:extractant ratios in mg/ml.

673
674

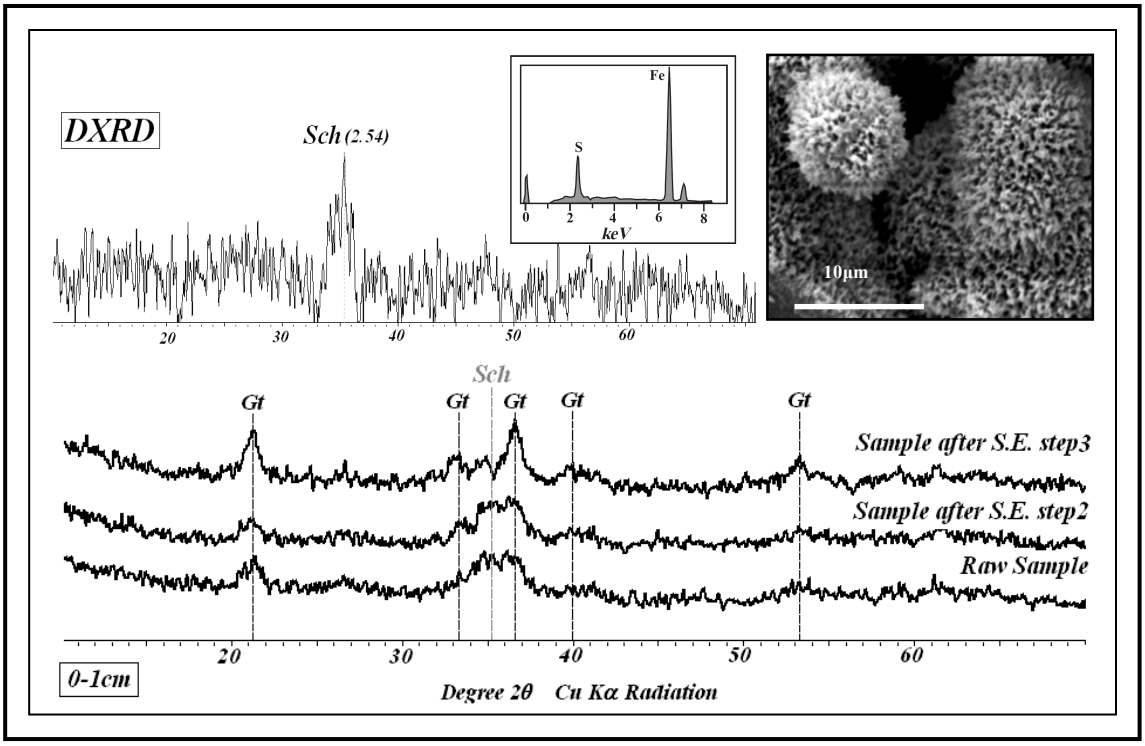

FIGURE 2. Mineralogical characterization of sample 0-1 cm by XRD, DXRD and SEM-EDS. Gt = Goethite, Sch = Schwertmannite.

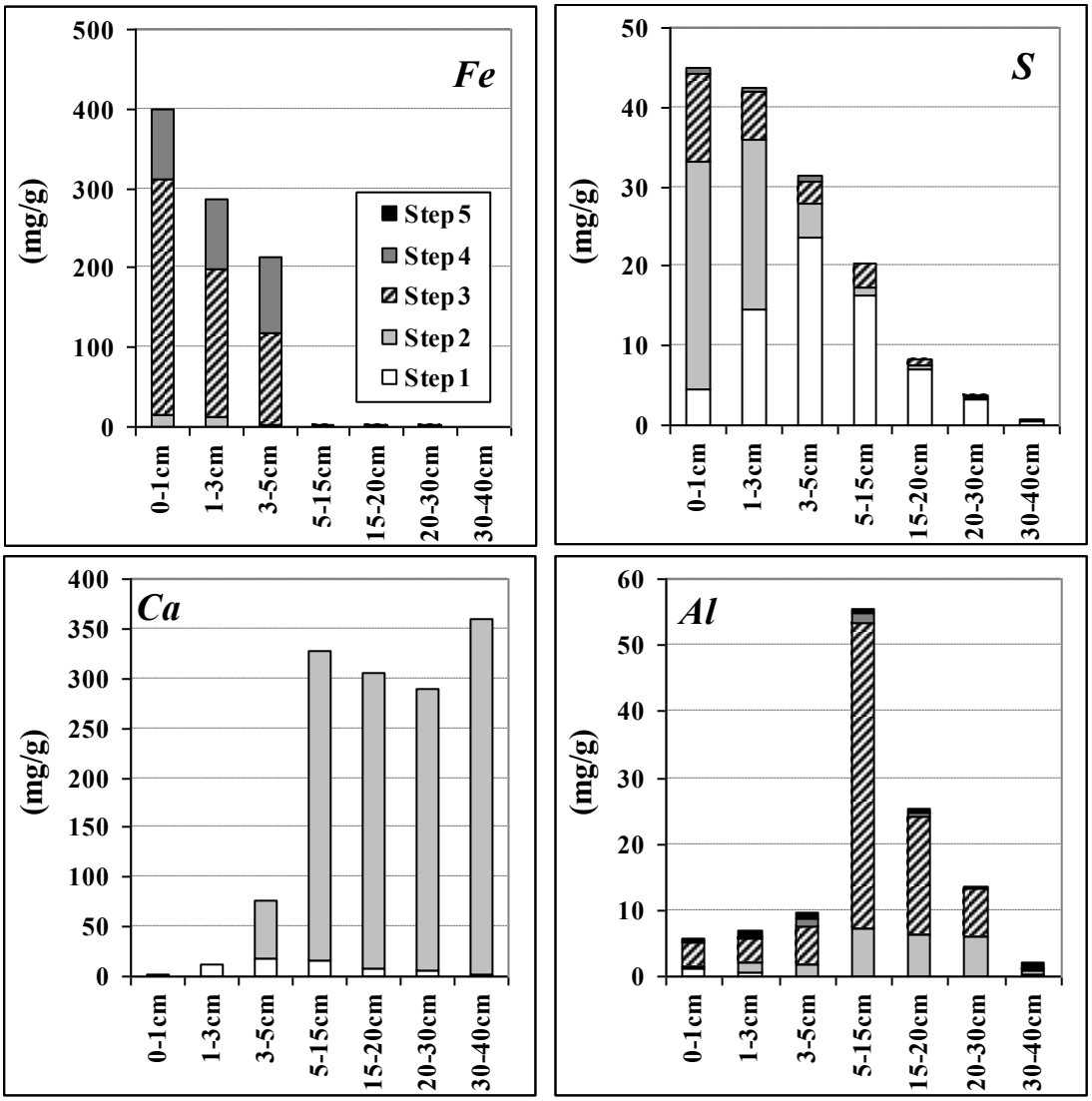

FIGURE 3. Distribution of Fe, Al, S and Ca concentrations throughout the sample profile on the basis of the sequential extraction study.

TABLE 2. Comparison between schwertmannite formula and $(Fe/S)_{molar}$ ratio proposed in the literature and schwertmannite formula and $(Fe/S)_{molar}$ ratio obtained in this study.

Sample	Fe (mmol/g) steps 2-3	S (mmol/g) steps 2-3	X value	Mineral formula	$(Fe/S)_{molar}$ ratio
Schwertmannite			$1^{*} \leq x \leq 1.86^{\#}$	$Fe_8O_8(OH)_{8-2x}(SO_4)_x$	4-8[§]
0-1cm	5.562	1.253	1.80	$Fe_8O_8(OH)_{4.39}(SO_4)_{1.8}$	4.44
1-3cm	3.576	0.861	1.93	$Fe_8O_8(OH)_{4.15}(SO_4)_{1.93}$	4.15
3-5cm	2.110	0.226	0.86	$Fe_8O_8(OH)_{6.28}(SO_4)_{0.86}$	9.33

X value correspond to the possible values of (SO_4) and (OH) in the schwertmannite compositional formula.
* (Bigham et al., 1996)
# (Yu et al., 1999)
§ (Bigham and Nordstrom, 2000)

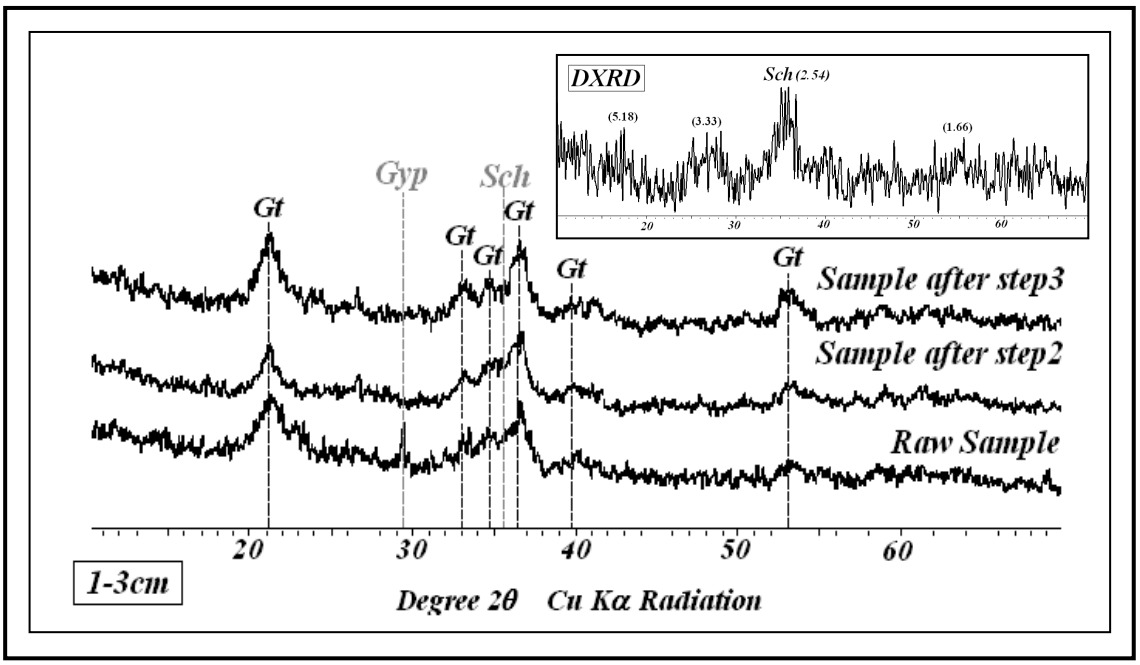

FIGURE 4. Mineralogical characterization by XRD and DXRD of sample 1-3 cm. Gt = Goethite, Sch = Schwertmannite, Gyp =Gypsum.

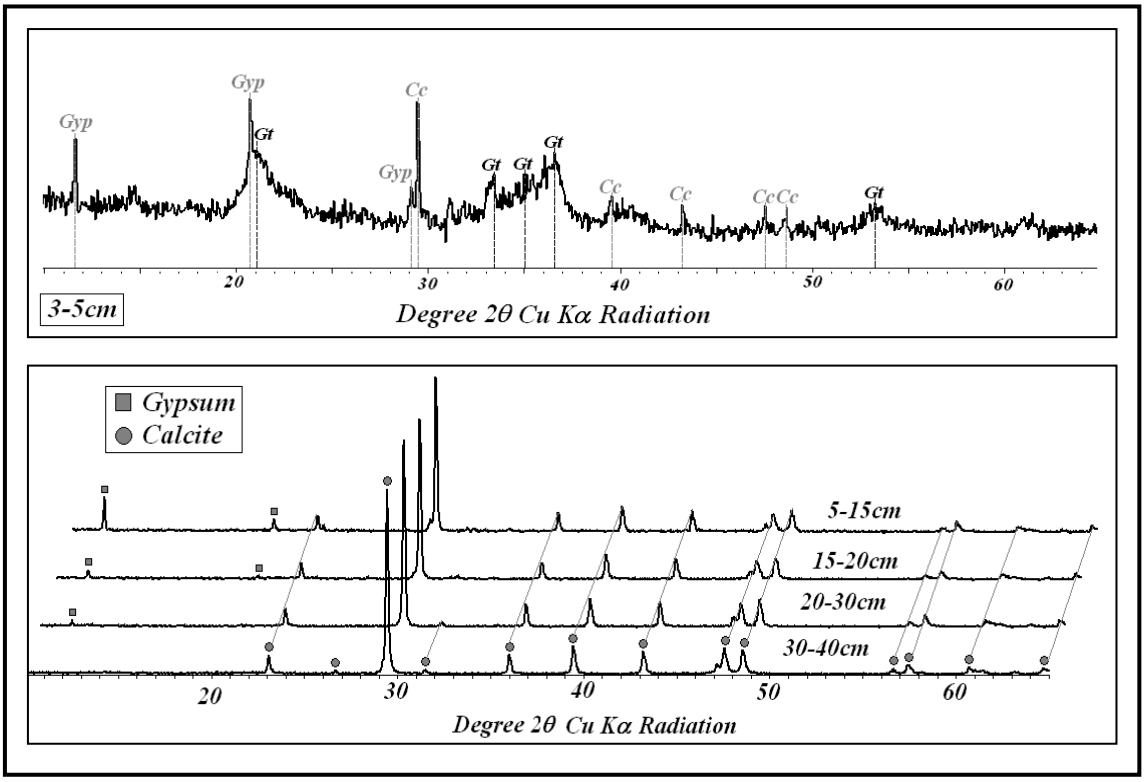

FIGURE 5. XRD diffractograms for samples from 3-5 cm and 30-40 cm. The most important peaks for the different mineral phases found in each sample have been labelled. Gt = Goethite, Gyp =Gypsum, Cc = Calcite.

TABLE 3. Deduced distribution of Al between hydrobasaluminite and gibbsite on the basis of steps 2-3 S and total Al.

Sample	S (mmol/g) steps 2-3	Al (mmol/g) total	Al (mmol/g) hybas*	Al (mmol/g) gibbsite #
5-15cm	0.127	2.026	0.507	1.519
15-20cm	0.041	0.910	0.164	0.746
20-30cm	0.018	0.498	0.071	0.427

* Al concentration calculated assuming all S from steps 2-3 corresponds to hydrobasaluminite $SO4_4^{=}$.
# Gibbsite Al concentration calculated by subtracting hydrobasaluminite Al concentration from total Al.

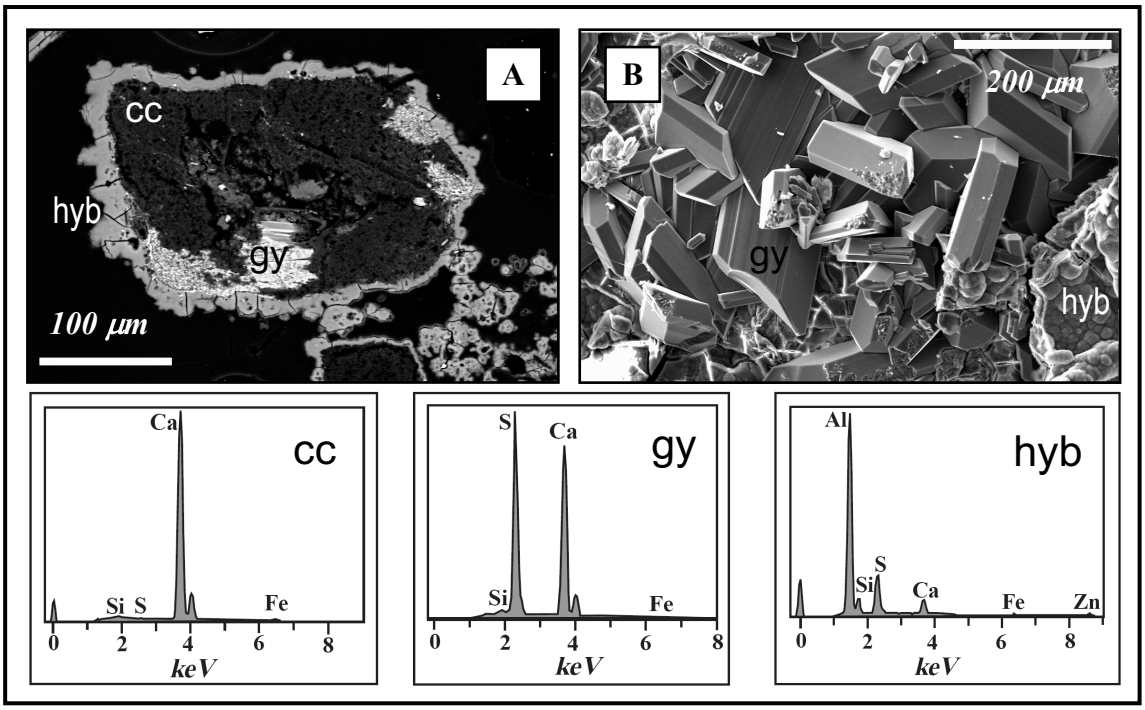

FIGURE 6. A) SEM image of a calcite grain surrounded by hydrobasaluminite (gray) and gypsum (bright white) precipitates. **B)** Euhedral crystals of gypsum (centre) and amorphous precipitates of hydrobasaluminite (lower-right corner of the image). At the bottom of these two images three EDS elemental spectra (calcite = "cc", gypsum = "gy", and hydrobasaluminite = "hyb") obtained for some of the detected minerals are shown.

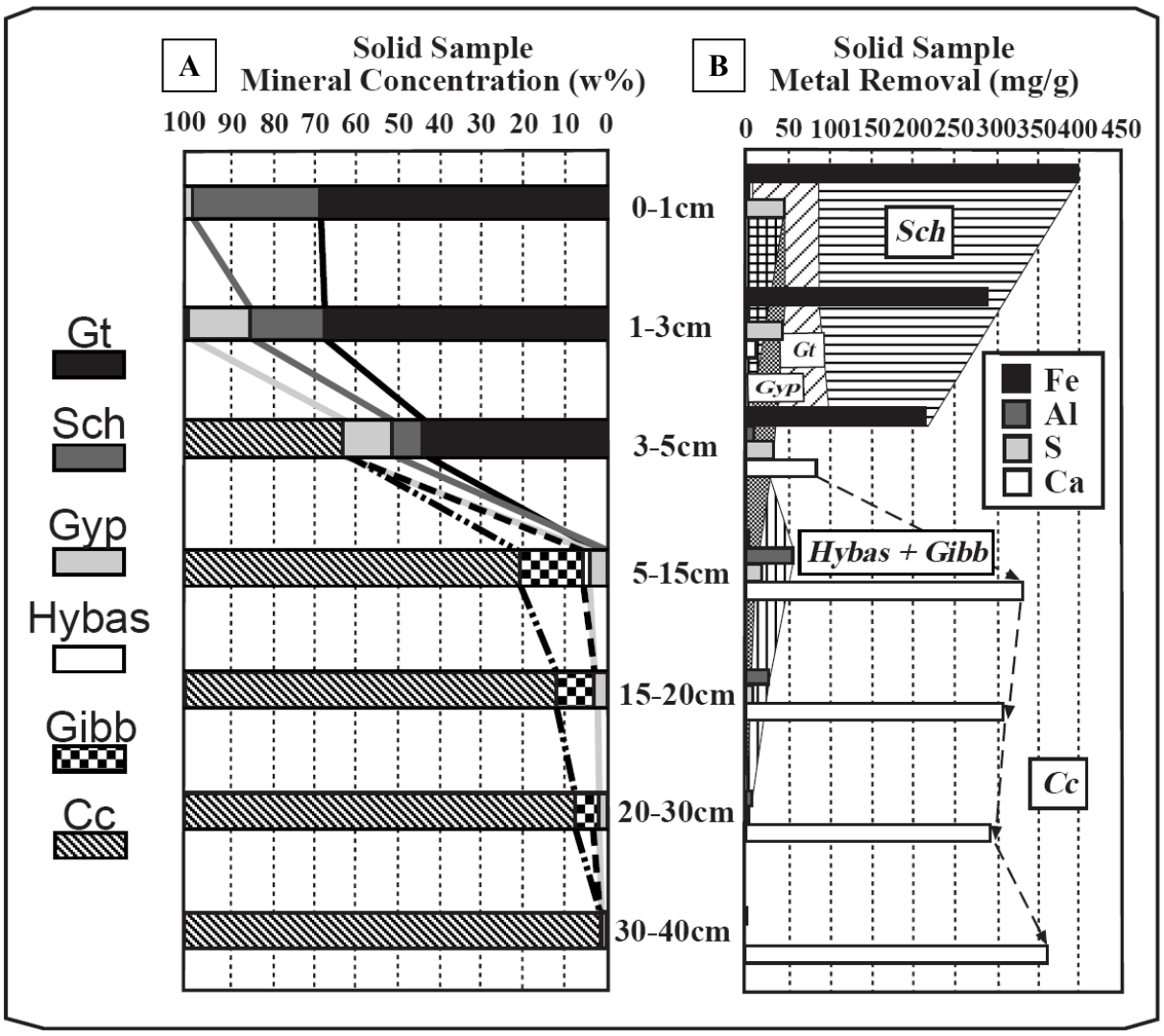

815

816 **FIGURE 7.** Metal (right diagram) and mineral (left diagram) distribution across the Monte Romero reactive tank profile. Gt = Goethite, Sch
817 = Schwertmannite, Gyp =Gypsum, Hybas = Hydrobasaluminite, Gibb = Gibbsite, Cc = Calcite. The different areas drawn on the right
818 diagram correspond to the amount of each element attributed to the individual mineral phases.

819